

# Nighttime Chemical Transformation in Biomass Burning Plumes: A Box Model Analysis Initialized with Aircraft Observations

Zachary C. J. Decker,<sup>†,‡,§,||</sup> Kyle J. Zarzana,<sup>†,§,◆</sup> Matthew Coggon,<sup>†,§,||</sup> Kyung-Eun Min,<sup>†,§,#</sup> Ilana Pollack,<sup>†,⊗</sup> Thomas B. Ryerson,<sup>§</sup> Jeff Peischl,<sup>†,§</sup> Pete Edwards,<sup>||</sup> William P. Dubé,<sup>†,§</sup> Milos Z. Markovic,<sup>†,⊙</sup> James M. Roberts,<sup>†,§</sup> Patrick R. Veres,<sup>§</sup> Martin Gaus,<sup>†,▽</sup> Carsten Warneke,<sup>†,§</sup> Joost de Gouw,<sup>†,‡,||</sup> Lindsay E. Hatch,<sup>⊥</sup> Kelley C. Barsanti,<sup>⊥,||</sup> and Steven S. Brown<sup>\*,†,§</sup>

<sup>†</sup>Cooperative Institute for Research in Environmental Sciences, University of Colorado, Boulder, Colorado 80309, United States

<sup>‡</sup>Department of Chemistry, University of Colorado, Boulder, Colorado 80309-0215, United States

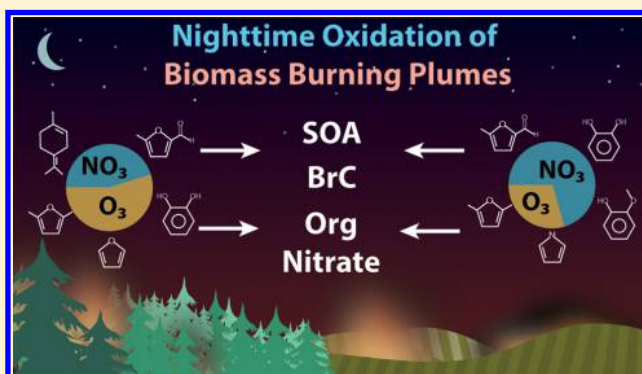
<sup>§</sup>NOAA Earth System Research Laboratory (ESRL), Chemical Sciences Division, Boulder, Colorado 80305, United States

<sup>||</sup>Wolfson Atmospheric Chemistry Laboratories, Department of Chemistry, University of York, York YO10 5DD, United Kingdom

<sup>⊥</sup>Department of Chemical and Environmental Engineering and College of Engineering – Center for Environmental Research and Technology (CE-CERT), University of California, Riverside, California 92507, United States

## Supporting Information

**ABSTRACT:** Biomass burning (BB) is a large source of reactive compounds in the atmosphere. While the daytime photochemistry of BB emissions has been studied in some detail, there has been little focus on nighttime reactions despite the potential for substantial oxidative and heterogeneous chemistry. Here, we present the first analysis of nighttime aircraft intercepts of agricultural BB plumes using observations from the NOAA WP-3D aircraft during the 2013 Southeast Nexus (SENEX) campaign. We use these observations in conjunction with detailed chemical box modeling to investigate the formation and fate of oxidants ( $\text{NO}_3$ ,  $\text{N}_2\text{O}_5$ ,  $\text{O}_3$ , and  $\text{OH}$ ) and BB volatile organic compounds (BBVOCs), using emissions representative of agricultural burns (rice straw) and western wildfires (ponderosa pine). Field observations suggest  $\text{NO}_3$  production was approximately  $1 \text{ ppbv hr}^{-1}$ , while  $\text{NO}_3$  and  $\text{N}_2\text{O}_5$  were at or below 3 pptv, indicating rapid  $\text{NO}_3/\text{N}_2\text{O}_5$  reactivity. Model analysis shows that  $>99\%$  of  $\text{NO}_3/\text{N}_2\text{O}_5$  loss is due to BBVOC +  $\text{NO}_3$  reactions rather than aerosol uptake of  $\text{N}_2\text{O}_5$ . Nighttime BBVOC oxidation for rice straw and ponderosa pine fires is dominated by  $\text{NO}_3$  (72, 53%, respectively) but  $\text{O}_3$  oxidation is significant (25, 43%), leading to roughly 55% overnight depletion of the most reactive BBVOCs and  $\text{NO}_2$ .



## INTRODUCTION

Wildfire size and frequency in the Western U.S. has increased over the last 20 years, and these trends are projected to continue due to factors such as forest management practices, elevated summer temperatures, earlier snowmelt, and drought.<sup>1,2</sup> Biomass burning (BB), including wildfires, prescribed burning, and agricultural burning, represents a large, imperfectly characterized, and chemically complex source of reactive material to the troposphere. BB releases reactive species and particulate matter that impact the radiative balance of the atmosphere, air quality, and human health on local to global scales.<sup>3–7</sup> The gas-phase components of BB plumes include volatile organic compounds (BBVOCs) as well as nitrogen oxides ( $\text{NO}_x = \text{NO} + \text{NO}_2$  and higher oxides such as peroxyacyl and alkyl nitrates), oxidants, and oxidant precursors. The air quality and climate effects of BB emissions are defined in part by the oxidative processes and atmospheric

chemical cycles that occur as the smoke is transported, diluted, and exposed to oxidants over the hours and weeks following emission.

The photochemistry of BB plumes has been studied previously in a number of field and laboratory studies. Daytime BB plumes can have  $\text{OH}$  concentrations 5–10 times higher than background air,<sup>8</sup> and daytime reactions of  $\text{NO}_x$ , BBVOCs, and  $\text{OH}$  involve complex pathways that generally lead to  $\text{O}_3$  formation, but in some cases to near-field  $\text{O}_3$  titration.<sup>9–14</sup> Much less is known about nighttime BB plume oxidative processes, which are expected to be dominated by nitrate radicals ( $\text{NO}_3$ ) and  $\text{O}_3$ .<sup>15</sup>  $\text{NO}_3$  is formed by  $\text{O}_3$  oxidation of

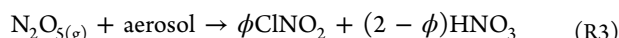
Received: September 24, 2018

Revised: January 22, 2019

Accepted: January 30, 2019

Published: January 30, 2019

$\text{NO}_x$  (eq R1 and Figure 1) but is rapidly ( $\tau < 10$  s) destroyed in the daytime by NO and photolysis.<sup>15,16</sup>  $\text{NO}_3$  is a precursor for  $\text{N}_2\text{O}_5$  (eq R2), a  $\text{NO}_x$  reservoir.  $\text{N}_2\text{O}_5$  may undergo heterogeneous uptake to form  $\text{ClNO}_2$  and  $\text{HNO}_3$  (eq R3). The former is a daytime Cl radical precursor affecting both marine and continental environments and influencing next-day  $\text{O}_3$  production.<sup>17–20</sup>  $\text{NO}_3$  can also be directly taken up onto aerosol (eq R4).



Mixing of background or smoke-derived<sup>14</sup>  $\text{O}_3$  with  $\text{NO}_x$  in a BB plume leads to the production of  $\text{NO}_3$ , which may be rapid ( $>0.5$  ppbv  $\text{h}^{-1}$ ). Recent laboratory measurements conducted during both the Fire Lab at Missoula Experiment (FLAME-4) and the ongoing Fire Influence on Regional and Global Environments Experiment (FIREX) have provided detailed identification and quantification of emissions for a range of BBVOCs.<sup>4,5,21–23</sup> Emissions inventories from these experiments indicate that the compounds emitted and their relative concentrations depend on the fuel type (e.g., pine vs grass), combustion process (e.g., smoldering or flaming), ignition procedure (e.g., fast or slow), and pyrolysis temperature (e.g., high or low).<sup>4,21,24,25</sup> Generally, primary BBVOC emissions include oxygenated hydrocarbons and aromatics (e.g., phenols) as well as unsaturated hydrocarbons, biogenic and hetero-aromatic species.<sup>4,5,21</sup> Many such compounds are very reactive toward  $\text{NO}_3$ <sup>26–33</sup> and may significantly limit its lifetime, promote secondary organic aerosol formation (SOA),<sup>34,35</sup> and alter nighttime oxidative budgets.

The coemission of  $\text{NO}_x$ , highly reactive VOCs, and aerosol particles leads to the potential for significant nighttime chemical transformations. Despite this potential, there has

been only one aircraft campaign to date from which sampling of nighttime biomass burning plumes has been reported.<sup>36,37</sup>

The Southeast Nexus (SENEX) campaign in 2013 included 20 research flights of an instrumented NOAA WP-3D aircraft, and one of the goals was to study the interactions between anthropogenic and biogenic emissions.<sup>38</sup> A night flight on July 2–3 targeted the emissions and nighttime chemistry from a power plant plume near the Mississippi river. During this flight, the WP-3D also targeted and intercepted agricultural BB plumes yielding the first airborne study of nighttime smoke that included  $\text{NO}_3$  and  $\text{N}_2\text{O}_5$  measurements.<sup>36</sup> Even so, there has been no previous analysis of BB  $\text{NO}_3$  chemistry using nighttime aircraft intercepts.

Here, we present the first analysis of nighttime smoke oxidation based on aircraft intercepts of fire plumes using data from this flight. With these observations, we initiate a detailed chemical box model to understand the chemical evolution of oxidants ( $\text{NO}_3$ ,  $\text{N}_2\text{O}_5$ ,  $\text{O}_3$ , and OH) and BBVOCs over one night (10 h) using emissions for rice straw to model a generic agricultural burning plume. We then use this analysis to model nighttime chemistry in western wildfires using emissions for a ponderosa pine fire.

**Field and Laboratory Measurements.** Field data for this study were taken from multiple instruments deployed on the NOAA WP-3D aircraft during the SENEX 2013<sup>38</sup> flight on July 2–3, 2013 (20:00–03:00 CDT). Our analysis utilizes data from the NOAA nitrogen oxide cavity ring-down spectrometer (CRDS) for  $\text{NO}_2$ ,  $\text{NO}_3$ ,  $\text{N}_2\text{O}_5$ , and  $\text{O}_3$ <sup>39–42</sup> as well as the  $\text{NO}_y\text{O}_3$  chemiluminescence instrument (CL) for NO,  $\text{NO}_2$ ,  $\text{O}_3$ , and  $\text{NO}_y$ <sup>43</sup> with 1 Hz acquisition resolution. Within the plume regions we study, the measurements of  $\text{NO}_2$  and  $\text{O}_3$  from the CRDS and CL instruments agree within 7%. We also use data from an ultrahigh sensitivity aerosol spectrometer (UHSAS) for aerosol size measurements (1 Hz)<sup>44,45</sup> and a proton-transfer-reaction mass spectrometer (PTR-MS) for VOC measurements (1 s every 17 s).<sup>46</sup>

BB intercepts were identified by the enhancement above background of four species: black carbon (BC), glyoxal (CHOCHO), CO, and acryloyl peroxyxynitrate (APAN).<sup>36,47</sup> BB identifier data were provided by the NOAA airborne cavity enhanced spectrometer (ACES)<sup>48</sup> for glyoxal, iodide chemical ionization mass spectrometer ( $\text{I}^-$  CIMS) for APAN,<sup>49</sup> single particle soot photometer (SP2) for black carbon,<sup>50</sup> and vacuum ultraviolet fluorimeter for CO.<sup>51</sup> Power plant plumes were identified by the above background enhancements of  $\text{NO}_x$  and  $\text{N}_2\text{O}_5$ . While CO is also present in the power plant plumes, the three other BB identifiers were not. Information on background and plume measurements is included in the Supporting Information (SI) (Tables S1 and S2).

Five VOCs (toluene, isoprene + furan, methylvinylketone + methacrolein (MVK + MACR), and methylethylketone (MEK)) as well as acetonitrile were measured by the PTR-MS during SENEX and overlap with our inventory. However, we explain in the SI that we do not use these observations because we do not know the fire source, number of fires, or fuel, and plume age estimates are highly uncertain (Figure S5).

Our detailed chemical box model uses emission inventories from Hatch et al.<sup>5</sup> and Koss et al.<sup>4</sup> for the ponderosa pine and rice straw fuels. The BBVOC emissions from Hatch et al.<sup>5,21</sup> were measured during FLAME-4 using the following instruments: two-dimensional gas chromatography–time-of-flight mass spectrometry, open-path Fourier-transform infrared gas spectroscopy,<sup>22</sup> whole-air sampling with one-dimensional gas

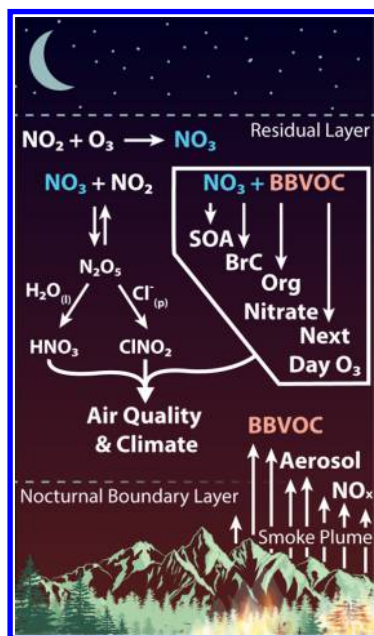


**Figure 1.** Schematic of nighttime  $\text{NO}_3$  and  $\text{N}_2\text{O}_5$  chemical processing in a biomass burning plume.

chromatography–mass spectrometry, and PTR time-of-flight mass spectrometry (PTR-ToF).<sup>52</sup> BBVOC emissions from Koss et al.<sup>4</sup> were measured by PTR-ToF during FIREX. Details regarding how the two inventories were merged are included in the SI. In general, for compounds shared between both inventories, the emission ratios (E1) agree within an order of magnitude with some exceptions (Figure S6). We propagate this variability into our model results (SI).

**Analysis and Modeling Methods.** We report our emissions in the form of laboratory-derived emission ratios (ER), which is the background subtracted emitted compound ( $x$ ) normalized to background subtracted CO.<sup>4,21</sup>

$$ER_x = \frac{x(\text{ppbv})}{\text{CO}(\text{ppmv})} \quad (\text{E1})$$

These emissions are integrated over the entirety of the laboratory fires and therefore contain emissions from all stages of the fire.

The modified combustion efficiency (MCE) was calculated for each plume.

$$\text{MCE} = \frac{\text{CO}_2 - \text{CO}_{2\text{bkg}}}{(\text{CO}_2 - \text{CO}_{2\text{bkg}}) + (\text{CO} - \text{CO}_{\text{bkg}})} \quad (\text{E2})$$

During plume intercepts, the average MCE was  $95 \pm 6\%$ , which is consistent with previous MCE calculations of the July 2–3 night flight.<sup>36</sup>

The total  $\text{NO}_3$  reactivity toward BBVOCs is given by

$$k_{\text{NO}_3}^{\text{BBVOC}} = \sum k_{\text{NO}_3 + \text{BBVOC}_i} [\text{BBVOC}_i] \quad (\text{E3})$$

where  $k_{\text{NO}_3 + \text{BBVOC}_i}$  is the bimolecular rate coefficient for  $\text{NO}_3 + \text{BBVOC}_i$  and  $k_{\text{NO}_3}^{\text{BBVOC}}$  is the pseudo-first order rate coefficient. The bimolecular rate coefficients for  $\text{NO}_3$ ,  $\text{O}_3$ , or  $\text{OH} + \text{BBVOC}$  were taken from literature where available and estimated by structure–activity relationships<sup>31,53</sup> or structural similarity where unavailable (SI).

Due to limited literature on  $\text{NO}_3 + \text{BBVOC}$  rate coefficients, our inventory excludes many nitriles, amines, alkynes, acids, and other compounds whose rate coefficients were unavailable and could not be estimated. We also removed saturated hydrocarbons because they are generally unreactive toward  $\text{NO}_3$ .<sup>28</sup> Despite this, our merged inventory retains about 87% of the total inventory carbon mass, or 96% by mass, with 235 compounds from Hatch et al.<sup>5</sup> and 171 compounds from Koss et al.<sup>4</sup> with 103 compounds shared in both inventories for a total of 303 unique compounds.

To calculate the observed  $\text{NO}_3$  reactivity during SENEX BB plume intercepts we determined BBVOC concentration using background corrected CO measured on the WP-3D.

$$\text{BBVOC}(\text{ppbv}) = ER_{\text{BBVOC}}(\text{CO} - \text{CO}_{\text{bkg}}) \quad (\text{E4})$$

As shown below, BBVOC is likely the main sink of  $\text{NO}_3$ ; therefore, the extent of BBVOC oxidation by  $\text{NO}_3$  will be limited by the  $\text{NO}_x/\text{BBVOC}$  ratio as  $\text{NO}_x$  is the source for  $\text{NO}_3$  (eq R1). Furthermore, the relative oxidative importance between  $\text{O}_3$  and  $\text{NO}_3$  depends on the  $\text{NO}_x/\text{BBVOC}$  ratio as explained by Edwards et al.<sup>54</sup> Therefore, in contrast to the method used for calculating BBVOC concentration in SENEX fire plume intercepts described above, we initiate our box model with fire emissions scaled to  $\text{NO}_x$  in order to preserve

the  $\text{NO}_x/\text{BBVOC}$  ratio observed during the fire lab experiments.

To estimate the emitted  $\text{NO}_x$  at the fire source, we assume that the total reactive nitrogen ( $\text{NO}_y$ , which does not include  $\text{NH}_3$ ) is equivalent to the emitted  $\text{NO}_x$ . The  $\text{NO}_x/\text{NO}_y$  ratio as measured during SENEX fire plume intercepts in Figure 2 was 0.84. We calculated the observed  $\text{NO}_y$  emission ratio using  $\text{NO}_y$  ( $13.2 \pm 3.1$  ppbv) and CO ( $543.4 \pm 87.7$  ppbv) enhancements above background. The calculated  $\text{NO}_y$  emission ratio, which we assume to be the  $\text{NO}_x$  emission ratio at the fire source, was determined to be  $24.3 \pm 6.4$  ppbv  $\text{NO}_y/\text{ppmv}$  CO for the plume intercept. We compared the estimated observed  $\text{NO}_x$  emission ratio to the  $\text{NO}_x$  emission ratios reported by Selimovic et al. for rice straw ( $43.9$  ppbv  $\text{NO}_x/\text{ppmv}$  CO) and ponderosa pine ( $26.9 \pm 4.3$  ppbv  $\text{NO}_x/\text{ppmv}$  CO).<sup>23</sup> We then scaled the BBVOC emissions by this ratio (E5), effectively scaling the fire emissions to the  $\text{NO}_x$  of the observed fire plume.

$$[\text{BBVOC}]^{\text{model}} = [\text{BBVOC}]^{\text{inventory}} \frac{ER_{\text{NO}_y}^{\text{obsd}}}{ER_{\text{NO}_x}^{\text{inventory}}} \quad (\text{E5})$$

The  $\text{NO}_x$  emission ratio observed during the SENEX fire plume intercepts in Figure 2 was 45% and 11% lower than the laboratory-derived  $\text{NO}_x$  emission ratio for rice straw and ponderosa pine fires, respectively. To correctly model the  $\text{NO}_3$

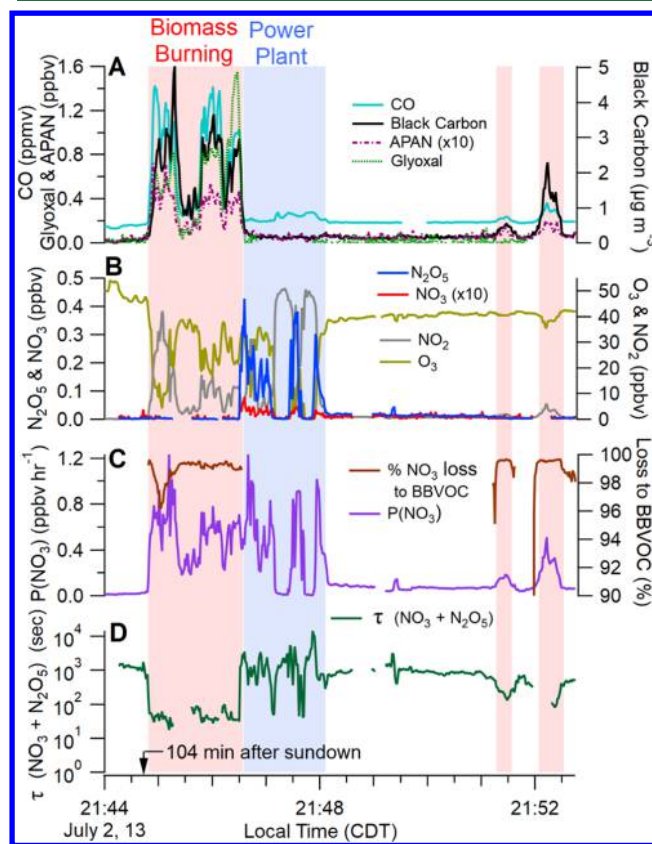


**Figure 2.** Time traces during representative sections of biomass burning (red) and power plant (blue) plume intercepts made 104 min after sundown ( $\text{SZA} = 90^\circ$ ): (A) BB tracers, (B)  $\text{NO}_3$ ,  $\text{N}_2\text{O}_5$ ,  $\text{NO}_2$ , and  $\text{O}_3$  mixing ratio, (C) production rate of  $\text{NO}_3$  and the percentage of  $\text{NO}_3$  loss to BBVOCs, (D) lifetime of  $\text{NO}_3$  and  $\text{N}_2\text{O}_5$ .



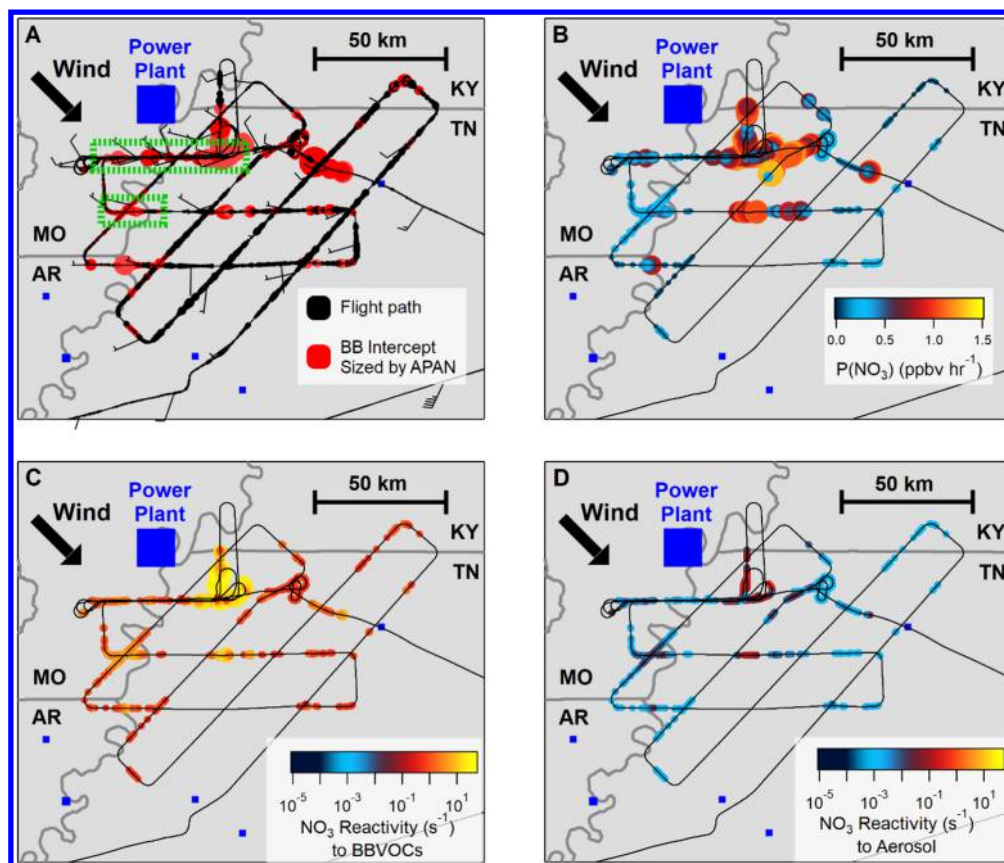


**Figure 3.** Flight maps of the SENEX July 2–3, 2013, night flight. (A) BB intercepts colored by red markers, sized by APAN (0.01–0.1 ppbv), and green dashes indicate sections shown in Figure 2. (B) Production rate of  $\text{NO}_3$ . (C, D) Comparisons of  $\text{NO}_3$  reactivity toward BBVOCs (C) and toward aerosol (D) on the same color and log scale.

oxidation of these fires we reduced our BBVOC emissions by a factor of 55% for rice straw and 89% for ponderosa pine.

Model background and initial concentrations of  $\text{NO}_x$ , CO, and  $\text{O}_3$  were taken from the SENEX observations shown in Figure 2. We estimate the NO/ $\text{NO}_2$  ratio at the fire source using the NO and  $\text{NO}_2$  emission ratios from FIREX for each fuel. The NO/ $\text{NO}_2$  ratios used are 5.3 and 2.8 for rice straw and ponderosa pine, respectively.<sup>23</sup> The background  $\text{NO}_2$  mixing ratio was taken to be 0.9 ppbv. The background  $\text{O}_3$  mixing ratio, 43.9 ppbv, was used as the starting  $\text{O}_3$  mixing ratio and is representative of the background  $\text{O}_3$  in the region where BB plumes were intercepted (Figure S3).

Box modeling was performed using the Framework for 0-D Atmospheric Modeling (FOAM)<sup>55</sup> to investigate the evolution of oxidized mass and oxidant fractions over 10 h (the approximate duration of one night in July in the Southeastern U.S.). Chemical mechanisms were adopted from the MCM (v3.3.1,<sup>56–60</sup> via <http://mcm.york.ac.uk>), and published mechanisms for methylguaiacol, syringol, *o*-guaiacol, and 3-methylfuran were added (Table S4).<sup>61–63</sup> Compounds not included in the above references were modeled as a one-step reaction of BBVOC +  $\text{NO}_3$ , BBVOC +  $\text{O}_3$ , or BBVOC + OH to form a single oxidation product.

All models were run at 298 K, typical experimental conditions for most published rate coefficients. Temperatures during flight ranged between 288 and 290 K (SI). In order to account for dilution processes, as well as entrainment of  $\text{O}_3$ , we apply a first order dilution of  $k_{\text{dil}} = 1.16 \times 10^{-5} \text{ s}^{-1}$  or a 24 h lifetime. The sensitivity of this assumption is shown in Figure

S2 and discussed in the SI. We report a base case model result with upper and lower bound uncertainties based on the emission and rate coefficient uncertainties, although, as discussed in the SI, the bounds do not provide information on the error distribution.

## RESULTS AND DISCUSSION

In panel A of Figure 2 the power plant plume intercepts (blue background) are distinguished from the fire plume intercepts (red background) by CO, black carbon, APAN, and glyoxal. Intercepts shown in Figure 2 were at an altitude between 700 and 900 m. Relative to the BB plume intercepts, the power plant plume intercepts exhibited elevated levels of  $\text{NO}_3$  and  $\text{N}_2\text{O}_5$  (Figure 2B). Figure 3A shows a flight map of the July 2–3 flight colored red during BB plume intercepts and sized by the APAN mixing ratio. Roughly 97% of the indicated BB plumes do not show signs of power plant plume mixing (SI). Green dashed boxes indicate sections of data shown in Figure 2.

The flight covered the intersection of Missouri, Kentucky, Tennessee, and Arkansas at the Mississippi river. According to the USDA CropScape database, this land is mainly agricultural, and therefore, the fire plume is most likely the result of burning crop residue and stubble.<sup>36,64</sup> Plume intercepts occurred near winter wheat crops and rice straw crops are situated roughly 70 km northwest. Still, rice straw is the best available fuel proxy for agricultural burning emissions. The wind direction was roughly northwesterly with most BB plume intercepts occurring in the northwest corner of Tennessee.

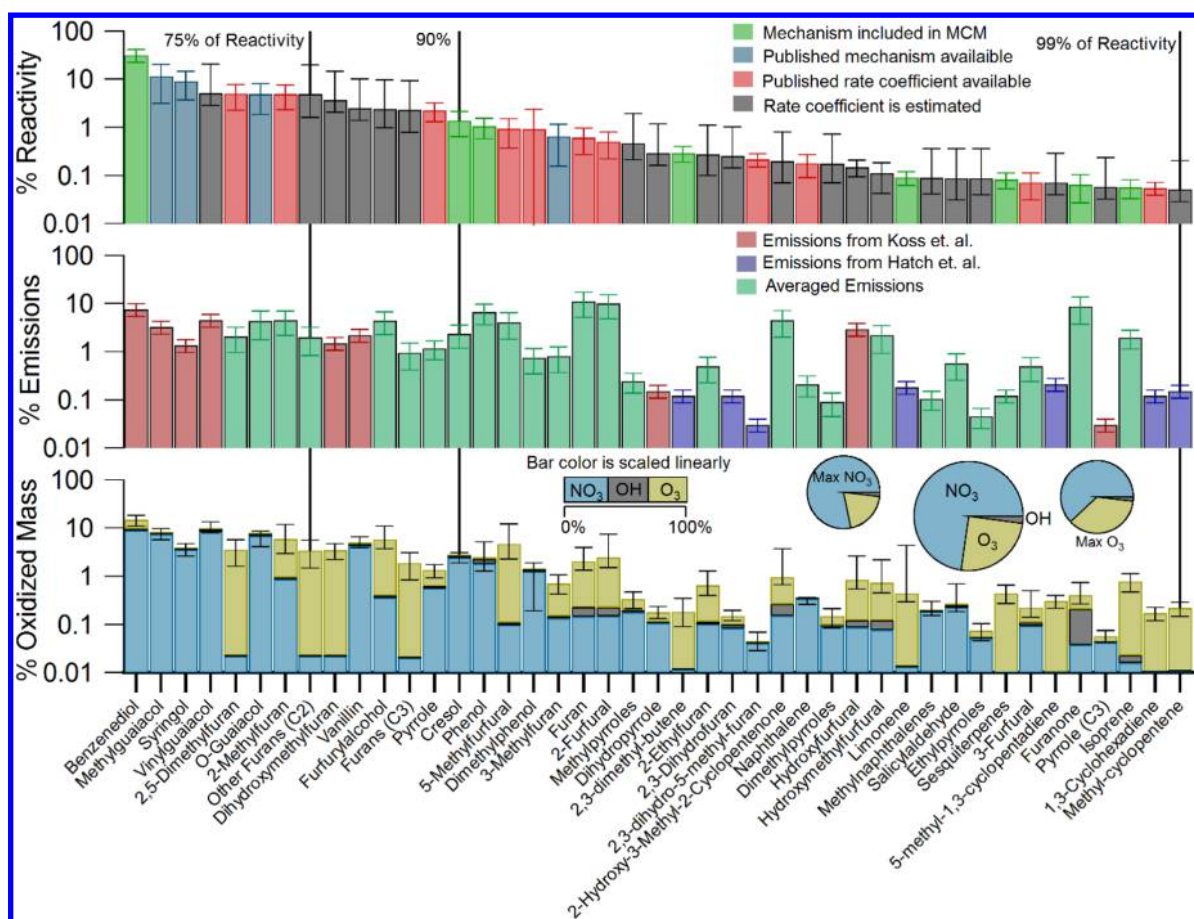


**Figure 4.** Rice straw fuel. The top panel shows the ranked order of the compounds that account for 99% of the rice straw initial NO<sub>3</sub> reactivity. The color scale describes the origin of the mechanisms or rate coefficient used. The middle panel is the relative BBVOC emission ratio normalized to the total BBVOC emission ratio, and the color scale describes the origin of the emissions data. The bottom panel is the relative nighttime reacted mass (10 h) normalized to total reacted mass. While the bar height is on a log scale, the color scale is linear and indicates the fraction of oxidation by NO<sub>3</sub> (blue), O<sub>3</sub> (gold), and OH (gray). The center pie chart shows the fraction of reacted mass in the base case with the maximum NO<sub>3</sub> oxidation case to the left and maximum O<sub>3</sub> oxidation case to the right. All panels sum to 100%.

To illustrate the NO<sub>3</sub> chemistry within a BB plume, we use previously published NO<sub>3</sub> and N<sub>2</sub>O<sub>5</sub> analysis metrics. The NO<sub>3</sub> production rate, P(NO<sub>3</sub>), is the instantaneous source of NO<sub>3</sub> from the reaction of NO<sub>2</sub> with O<sub>3</sub> and is given in (E6).<sup>15</sup> The NO<sub>3</sub> + N<sub>2</sub>O<sub>5</sub> lifetime ( $\tau$ ) is the ratio of NO<sub>3</sub> and N<sub>2</sub>O<sub>5</sub> concentration to the NO<sub>3</sub> production rate (E7).<sup>65</sup> The summed lifetime is useful because NO<sub>3</sub> and N<sub>2</sub>O<sub>5</sub> reach an equilibrium state that is typically more rapid than the individual sink reactions for either, such that they can be regarded as a sum.

$$P(\text{NO}_3) = k_{\text{NO}_3}[\text{NO}_2][\text{O}_3] \quad (\text{E6})$$

$$\tau(\text{NO}_3 + \text{N}_2\text{O}_5) = \frac{[\text{NO}_3] + [\text{N}_2\text{O}_5]}{P(\text{NO}_3)} \quad (\text{E7})$$

P(NO<sub>3</sub>) was large and of similar magnitude in both the power plant plume and BB plume (Figure 2C). Figure 3B is colored by NO<sub>3</sub> production during BB intercepts only, and shows that large NO<sub>3</sub> production rates, near 1 ppbv hr<sup>-1</sup>, were observed during multiple BB plume intercepts. Despite the large NO<sub>3</sub> radical production, the NO<sub>3</sub> and N<sub>2</sub>O<sub>5</sub> concentrations within the BB plume were below the 3 pptv<sup>38</sup> stated detection limit of the instrument (Figure 2B), yielding short NO<sub>3</sub> + N<sub>2</sub>O<sub>5</sub> lifetimes. Indeed, as shown in Figure 2D,  $\tau$  is roughly a factor of 100 lower within the BB plume as

compared to the power plant plume and background air. Because the NO<sub>3</sub> and N<sub>2</sub>O<sub>5</sub> were below stated detection limits in the BB plumes, the corresponding lifetimes shown in Figure 2D are upper limits, and the actual lifetimes may be considerably shorter.

The high production rate and short lifetime of NO<sub>3</sub> + N<sub>2</sub>O<sub>5</sub> within the BB plume is evidence for rapid NO<sub>3</sub> or N<sub>2</sub>O<sub>5</sub> loss pathways. BB plumes contain large quantities of both aerosol and BBVOCs, which provide two efficient NO<sub>3</sub>/N<sub>2</sub>O<sub>5</sub> loss pathways. To understand the competition between these loss processes, we calculated an instantaneous NO<sub>3</sub> reactivity toward aerosol and toward BBVOCs. The total NO<sub>3</sub> loss to BBVOC is calculated using the sum of BBVOC reactivity normalized to CO (E3). The total NO<sub>3</sub> loss to aerosol uptake is given as the sum of both NO<sub>3</sub> and N<sub>2</sub>O<sub>5</sub> uptake rate coefficients. By assuming a steady state<sup>66</sup> for both NO<sub>3</sub> and N<sub>2</sub>O<sub>5</sub>, we estimate the total aerosol uptake, and therefore NO<sub>3</sub> reactivity toward aerosol, as

$$k_{\text{NO}_3}^{\text{aerosol}} = K_{\text{eq}}[\text{NO}_2]k_{\text{N}_2\text{O}_5+\text{aerosol}} + k_{\text{NO}_3+\text{aerosol}} \quad (\text{E8})$$

where  $k_{\text{NO}_3}^{\text{aerosol}}$  is a first-order rate coefficient,  $K_{\text{eq}}$  is the equilibrium constant between NO<sub>3</sub> and N<sub>2</sub>O<sub>5</sub> (R2), and  $k_{\text{x}+\text{aerosol}}$  is the first order rate coefficient for N<sub>2</sub>O<sub>5</sub> or NO<sub>3</sub> aerosol uptake expressed below.



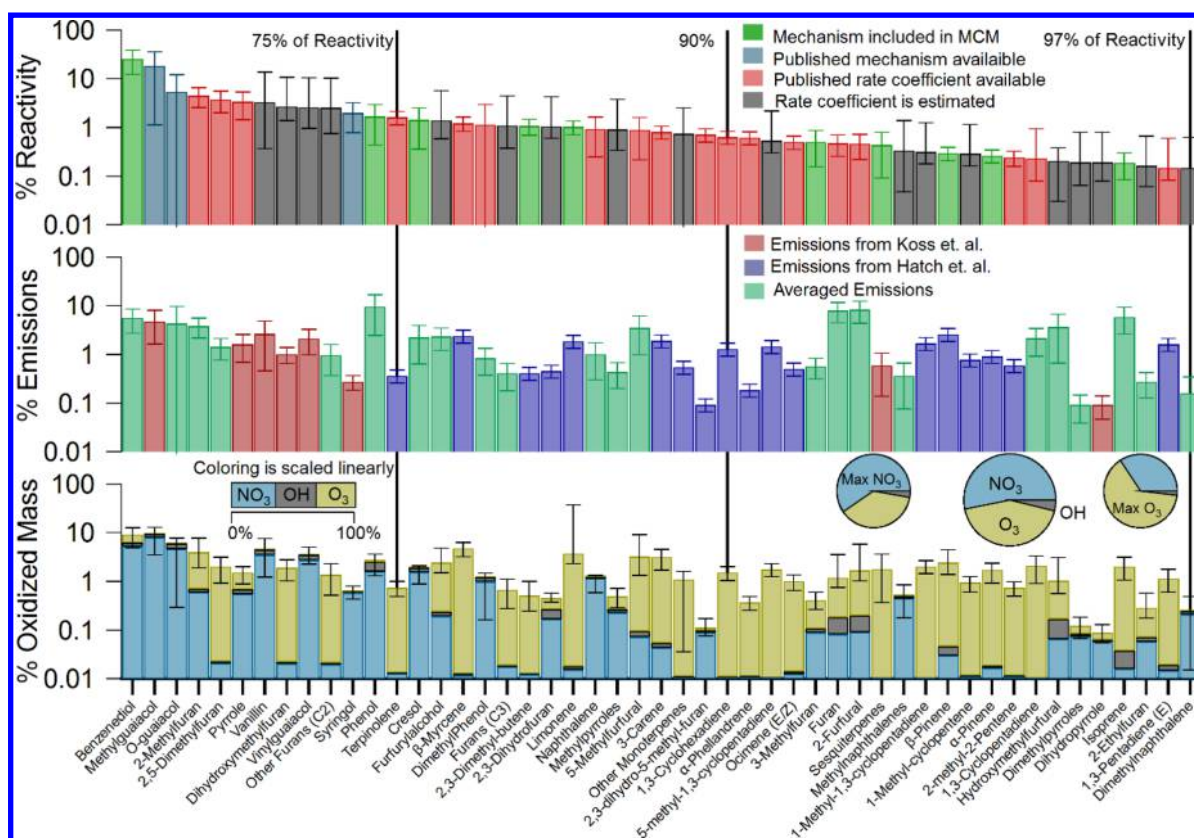


**Figure 5.** Same as Figure 4 but for ponderosa pine fuel. In the bottom panel the bar height is on a log scale, but the color scale is linear and indicates the fraction of oxidation by  $\text{NO}_3$  (blue),  $\text{O}_3$  (gold), and  $\text{OH}$  (gray).

$$k_{x+\text{aerosol}} = \frac{\gamma \bar{c} SA}{4} \quad (\text{E9})$$

Here,  $\gamma$  is the aerosol uptake coefficient,  $\bar{c}$  is the mean molecular speed, and  $SA$  is the aerosol surface area. Calculations use uptake coefficients of  $\gamma_{\text{N}_2\text{O}_5} = 10^{-2}$  for  $\text{N}_2\text{O}_5$ <sup>19</sup> and  $\gamma_{\text{NO}_3} = 10^{-3}$  for  $\text{NO}_3$ . However,  $\gamma_{\text{NO}_3}$  values have a wide range; therefore, we include calculations with  $\gamma_{\text{NO}_3} = 1$  in the SI but find similar results.<sup>15</sup>

Parts C and D of Figure 3 compare the  $\text{NO}_3$  reactivity toward BBVOCs and aerosol uptake during BB plume intercepts, respectively. In all BB intercepts, the calculated  $\text{NO}_3$  reactivity toward BBVOCs is a factor of 100–1000 greater than aerosol uptake. Figure 2C shows the percentage of  $\text{NO}_3$  reactivity dominated by BBVOC with a median >99%.

To understand which BBVOCs may be responsible for the rapid initial loss of  $\text{NO}_3$ , we calculated the relative  $\text{NO}_3$  reactivity for 303 compounds in rice straw and ponderosa pine burning emissions. The top panel of Figure 4 shows the ranked order of the compounds that account for 99% of the rice straw initial  $\text{NO}_3$  reactivity. Eight furan or phenol compounds are responsible for 75% of the initial  $\text{NO}_3$  reactivity. Most of the initial  $\text{NO}_3$  reactivity for a rice straw fire is accounted for by phenols ( $60^{+20}_{-14}\%$ ) and furans ( $23^{+20}_{-6}\%$ ), as well as pyrroles and furfurals ( $8^{+9}_{-3}\%$  combined).

The top panel of Figure 5 shows the ranked order of the compounds that account for 97% of the ponderosa pine initial  $\text{NO}_3$  reactivity. The top 75% of initial  $\text{NO}_3$  reactivity is distributed among 13 compounds with phenols ( $62^{+27}_{-23}\%$ ), furans ( $18^{+12}_{-4}\%$ ), and pyrrole and furfural ( $8^{+8}_{-3}\%$  combined) again dominating the total reactivity. Unlike rice straw, a

ponderosa pine fire plume has significant reactivity toward terpenes ( $8^{+2}_{-1}\%$ ). The initial  $\text{NO}_3$  reactivity toward terpenes and unsaturated hydrocarbons in a rice straw plume is <1%. These differences in reactivity are due to differences in emissions between the two fuels as explained below.<sup>5</sup>

The middle panels of Figures 4 and 5 show the emission ratios for each compound normalized to total emissions. The color indicates the origin of the emission ratio. The rice straw fire emissions for compounds included in Figure 4 are mainly furans ( $33 \pm 8\%$ ), phenols ( $27 \pm 4\%$ ), and furfurals ( $24 \pm 6\%$ ), while unsaturated hydrocarbon and terpene emissions account for only  $3 \pm 1\%$ . In contrast, the ponderosa pine fire emissions have a larger representation of terpenes ( $18 \pm 4\%$ ) and unsaturated hydrocarbons ( $10 \pm 2\%$ ), but phenols ( $33 \pm 10\%$ ), furans ( $17 \pm 4\%$ ), and furfurals ( $18 \pm 6\%$ ) are all still significant.

To better understand smoke plume evolution and to determine the amount of BBVOC mass oxidized during one night (10 h), we ran a 0-D box model for both rice straw and ponderosa pine fire emissions.  $\text{NO}_3$  and  $\text{N}_2\text{O}_5$  remained below 3 pptv (Figure S1), consistent with field observations (Figure 2B). Figure S1 illustrates that the summed concentrations of the most reactive BBVOCs are comparable to  $\text{NO}_2$ , suggesting there is approximately as much  $\text{NO}_3$  precursor available as there is BBVOC to be oxidized. For both fuels, roughly 50–60% of  $\text{NO}_2$  and the BBVOC compounds listed in Figure 4 and Figure 5 are depleted by chemistry (excluding dilution) in one night. Our box-model suggests several abundant BBVOCs survive the night with more than 50% of their initial starting concentration, such as phenol, furan, furfural, and hydroxymethylfurfural (SI).

HNO<sub>3</sub> production is complex within the model, and both maximum and minimum uncertainty bounds on HNO<sub>3</sub> concentrations are the result of higher bound BBVOC emissions, but lower and higher bound BBVOC rate coefficients, respectively. HNO<sub>3</sub> is the product of reactions of phenolic compounds with NO<sub>3</sub>, which proceeds by H-abstraction. HNO<sub>3</sub> production is dominated by catechol + NO<sub>3</sub> (~60%) within the first few hours, but as the more reactive compounds are depleted, the lesser reactive compounds like methyl guaiacol, guaiacol, and syringol react with NO<sub>3</sub> and dominate in the last 2 h. HNO<sub>3</sub> may be lost to the particle phase with concurrent NH<sub>3</sub> emission or other nitrogen species; however, this loss mechanism is not included in our model.

For both fuels, catechol is the most reactive compound, and accounts for 32 ± 9% and 26 ± 13% of initial NO<sub>3</sub> reactivity at the start of the simulation for rice straw and ponderosa pine plumes, respectively. However, Koss et al.<sup>4</sup> were unable to distinguish between catechol and methylfurfural at *m/z* = 110.1 We assume a 50/50 contribution here, which yields catechol emission ratios of 2.5 ± 0.8 ppbv ppmv<sup>-1</sup> CO for rice straw and 1.5 ± 0.6 ppbv ppmv<sup>-1</sup> CO for ponderosa pine. Still, the high reactivity is mainly due to the large catechol rate coefficient (9.9 × 10<sup>-11</sup> cm<sup>3</sup> molecule<sup>-1</sup> s<sup>-1</sup>),<sup>67</sup> which is the third greatest among the emitted compounds. Catechol is known to react with NO<sub>3</sub> by H-abstraction, with subsequent addition of NO<sub>2</sub> to the aromatic peroxy radical to form 4-nitrocatechol with a near-unity molar yield of 0.91 ± 0.06.<sup>68</sup> Further, 4-nitrocatechol is expected to almost completely (96%) partition to the particle phase.<sup>68</sup> Recently, Hartikainen et al.<sup>25</sup> investigated dark oxidation of residential wood combustion and found strong correlations between the depletion of phenolic compounds and the formation of NO<sub>3</sub>-initiated SOA. In wintertime BB events, 4-nitrocatechol and other derivatives have been detected in aerosol and are considered important light-absorbing components of brown carbon (BrC).<sup>35,69–76</sup>

SOA yields are a function of mass loadings.<sup>77</sup> Using a catechol mass loading of 300 μg m<sup>-3</sup> from Finewax et al.<sup>68</sup> as well as a total observed aerosol plume measurement of 58.7 μg m<sup>-3</sup>, we estimate a 4-nitrocatechol SOA mass yield of 120%. Assuming 0.6 ppbv of catechol in ponderosa pine and 0.8 ppbv in rice straw (initial model conditions) with 44 ppbv O<sub>3</sub>, 13 ppbv of NO<sub>x</sub> and *k*<sub>dil</sub> = 1.16 × 10<sup>-5</sup> s<sup>-1</sup>, we estimate the SOA produced from catechol to be 3.8 ± 1.0 μg m<sup>-3</sup> in 8 h and 4.0<sup>+1.1</sup><sub>-1.0</sub> μg m<sup>-3</sup> in 8.5 h for a rice straw and ponderosa pine plume, respectively. Further, there is evidence to suggest furans and furfurals may also be a source of SOA precursors.<sup>5,25</sup>

The bottom panel of Figure 4 shows the reacted mass per compound normalized to the total reacted mass. The bar height is on a log scale, but the bar color is linearly scaled and indicates the fraction of nighttime oxidation by NO<sub>3</sub> (blue), O<sub>3</sub> (gold), and OH (gray) after 10 h for each compound. The center pie chart in Figure 4 and 5 represents the base case fraction of reactant mass oxidized by each oxidant. The left and right pie charts show results for the estimated maximum possible NO<sub>3</sub> and maximum possible O<sub>3</sub> oxidation, respectively. Uncertainty in the fraction of oxidized mass is calculated from the uncertainties in individual compound emissions and rate coefficients. For the compounds comprising a rice straw BB plume, the majority of mass is oxidized by NO<sub>3</sub> (72<sup>+6</sup><sub>-11</sub>%). This is expected because the rice straw fuel emissions are rich in oxygenated aromatic and heteroaromatic emissions, which

are generally less reactive toward O<sub>3</sub>. Terpenes and unsaturated hydrocarbons, which are a small fraction of emissions in Figure 4, are relatively more reactive toward O<sub>3</sub>. Even so, O<sub>3</sub> still has a significant oxidative impact and is responsible for 26<sup>+11</sup><sub>-6</sub>% of oxidized BBVOC mass.

The relative amount of oxidized mass for ponderosa pine is shown in the bottom panel of Figure 5. Almost half of the oxidized mass for compounds included in Figure 5 is due to O<sub>3</sub> (43<sup>+21</sup><sub>-6</sub>%) for our base case. The phenolic compounds mainly undergo NO<sub>3</sub> oxidation while terpenes and unsaturated hydrocarbons are mainly oxidized by O<sub>3</sub>. Furans and the heteroaromatics are oxidized approximately evenly by O<sub>3</sub> and NO<sub>3</sub>. The increased fraction of O<sub>3</sub> oxidation is the result of the increased fraction of unsaturated hydrocarbon and terpenes in the ponderosa pine emissions when compared to rice straw.

The nighttime chemical evolution and oxidation products of a biomass burning plume will depend on the relative NO<sub>3</sub> and O<sub>3</sub> reactivity. Neglecting the small contribution from OH oxidation, Edwards et al.<sup>54</sup> show the competition between NO<sub>3</sub> and O<sub>3</sub> oxidation of biogenic VOCs (BVOC) is dependent on the NO<sub>x</sub>/BVOC ratio. We scaled our BBVOC emissions to maintain the NO<sub>x</sub>/BBVOC ratio expected for rice straw (0.4 ± 0.1) or ponderosa pine (0.3 ± 0.1) emissions. However, because fires are highly variable, the NO<sub>x</sub>/BBVOC ratio for any given fuel may vary from fire to fire. For rice straw, a factor of 2 increase in NO<sub>x</sub> increases the fraction of NO<sub>3</sub> oxidation from 72% to 84%, while a factor of 2 decrease in NO<sub>x</sub> decreases relative NO<sub>3</sub> oxidation to 55%. Similarly, for ponderosa pine, doubling NO<sub>x</sub> increases the fraction of NO<sub>3</sub> oxidation from 53% to 66%, while halving NO<sub>x</sub> decreases relative NO<sub>3</sub> oxidation to 37% and increases O<sub>3</sub> to 57%. Furthermore, we find that a factor of 2 change in ambient O<sub>3</sub> concentration has little effect on the relative NO<sub>3</sub> and O<sub>3</sub> reactivity (see the SI).

Our reactivity calculations and box-model results are most limited by a lack of kinetic and mechanistic studies for O<sub>3</sub>, NO<sub>3</sub>, and OH + BBVOCs reactions. Kinetic and mechanistic studies of furan, furfural, phenol, and pyrrole analogues reacting with NO<sub>3</sub> will be most critical to understanding nighttime BB processes, which we highlight in the SI.

The time of day in which a fire is active will determine the fate of its emissions. This paper presents the first nighttime aircraft intercepts of a BB plume combined with an inventory of 303 BBVOC emissions and an oxidation model to predict the lifetime and fate of BB emissions in the dark. Fire emissions at times near sunset will undergo the chemistry we have detailed here, which suggests a roughly 60% depletion (for both rice straw and ponderosa pine) of fire-derived NO<sub>x</sub>. We find that nighttime chemistry is likely to proceed by NO<sub>3</sub>, rather than N<sub>2</sub>O<sub>5</sub>, further slowing the loss of NO<sub>x</sub> (eqs R1 and R2). Our model applies to chemistry at the center of a plume and does not include dispersion. Dispersion mixes NO<sub>x</sub> with background O<sub>3</sub> at the edges of the plume leading to faster depletion, and therefore, the values we report are likely lower limits. Even so, 18–19% of BBVOC mass, out of the total BBVOC mass that we model, will be oxidized in one night. That is roughly a 55% depletion of the BBVOCs that are reactive toward NO<sub>3</sub>. There is evidence that many of these NO<sub>3</sub> reactive compounds can form secondary BrC aerosol,<sup>35,69–76</sup> suggesting nighttime oxidation may be a significant source of BB derived BrC. Furthermore, future BB photochemical models should consider that these reactive phenolic-, furan-, and furfural-like compounds are not only reactive

toward NO<sub>3</sub>, but also O<sub>3</sub> and OH, thus affecting next-day BB photochemistry.

## ■ ASSOCIATED CONTENT

### Supporting Information

The Supporting Information is available free of charge on the ACS Publications website at DOI: [10.1021/acs.est.8b05359](https://doi.org/10.1021/acs.est.8b05359).

Figure S1, box model time traces of key species; Figure S2, box model sensitivity to the dilution rate coefficient; Figure S3, correlation of O<sub>3</sub> and NO<sub>2</sub> from aircraft observations; Figure S4, altitude profiles of key species and potential temperature; Figure S5, plume age estimates; Figure S6, variability in emission ratios; Table S1, BB plume and background values; Table S2, plume and background times; Table S3, list of reactions excluded from the MCM; Table S4, mechanisms added to the MCM (PDF)

## ■ AUTHOR INFORMATION

### Corresponding Author

\*E-mail: [steven.s.brown@noaa.gov](mailto:steven.s.brown@noaa.gov).

### ORCID

Zachary C. J. Decker: 0000-0001-9604-8671

Matthew Coggon: 0000-0002-5763-1925

Joost de Gouw: 0000-0002-0385-1826

Kelley C. Barsanti: 0000-0002-6065-8643

### Present Addresses

◆(K.J.Z.) Department of Chemistry, University of Colorado, Boulder, Colorado 80309-0215, United States.

#(K.-E.M.) Gwangju Institute of Science and Technology, School of Earth Sciences and Environmental Engineering, Gwangju 61005, South Korea.

⊗(I.P.) Colorado State University, Atmospheric Science Department, Ft. Collins, CO 80523-1371.

○(M.Z.P.) Picarro, Inc., Santa Clara, CA 95054.

∇(M.G.) Department of Atmospheric and Cryospheric Sciences, University of Innsbruck, Innsbruck 6020, Austria.

### Notes

The authors declare no competing financial interest.

## ■ ACKNOWLEDGMENTS

We thank Charles A. Brock for aerosol surface area measurements.

## ■ REFERENCES

(1) Dennison, P. E.; Brewer, S. C.; Arnold, J. D.; Moritz, M. A. Large Wildfire Trends in the Western United States, 1984–2011. *Geophys. Res. Lett.* **2014**, *41*, 2928.

(2) Westerling, A. L.; Hidalgo, H. G.; Cayan, D. R.; Swetnam, T. W. Warming and Earlier Spring Increase Western U.S. Forest Wildfire Activity. *Science (Washington, DC, U. S.)* **2006**, *313* (5789), 940–943.

(3) Pope, C. A.; Dockery, D. W. Health Effects of Fine Particulate Air Pollution: Lines That Connect. *J. Air Waste Manage. Assoc.* **2006**, *56* (6), 709–742.

(4) Koss, A. R.; Sekimoto, K.; Gilman, J. B.; Selimovic, V.; Coggon, M. M.; Zarzana, K. J.; Yuan, B.; Lerner, B. M.; Brown, S. S.; Jimenez, J. L.; Krechmer, J.; Roberts, J. M.; Warneke, C.; Yokelson, R. J.; de Gouw, J. Non-Methane Organic Gas Emissions from Biomass Burning: Identification, Quantification, and Emission Factors from PTR-ToF during the FIREX 2016 Laboratory Experiment. *Atmos. Chem. Phys.* **2018**, *18* (5), 3299–3319.

(5) Hatch, L. E.; Yokelson, R. J.; Stockwell, C. E.; Veres, P. R.; Simpson, I. J.; Blake, D. R.; Orlando, J. J.; Barsanti, K. C. Multi-Instrument Comparison and Compilation of Non-Methane Organic Gas Emissions from Biomass Burning and Implications for Smoke-Derived Secondary Organic Aerosol Precursors. *Atmos. Chem. Phys.* **2017**, *17* (2), 1471–1489.

(6) Rotstayn, L. D.; Penner, J. E. Indirect Aerosol Forcing, Quasi Forcing, and Climate Response. *J. Clim.* **2001**, *14* (13), 2960–2975.

(7) Andreae, M. O.; Merlet, P. Emission of Trace Gases and Aerosols from Biomass Burning. *Global Biogeochem. Cycles* **2001**, *15* (4), 955–966.

(8) Yokelson, R. J.; Crouse, J. D.; DeCarlo, P. F.; Karl, T.; Urbanski, S.; Atlas, E.; Campos, T.; Shinzuka, Y.; Kapustin, V.; Clarke, A. D.; Weinheimer, A.; Knapp, D. J.; Montzka, D. D.; Holloway, J.; Weibring, P.; Flocke, F.; Zheng, W.; Toohey, D.; Wennberg, P. O.; Wiedinmyer, C.; Mauldin, L.; Fried, A.; Richter, D.; Walega, J.; Jimenez, J. L.; Adachi, K.; Buseck, P. R.; Hall, S. R.; Shetter, R. Emissions from Biomass Burning in the Yucatan. *Atmos. Chem. Phys.* **2009**, *9* (15), 5785–5812.

(9) Hennigan, C. J.; Sullivan, A. P.; Collett, J. L.; Robinson, A. L. Levoglucosan Stability in Biomass Burning Particles Exposed to Hydroxyl Radicals. *Geophys. Res. Lett.* **2010**, *37* (9), 1–4.

(10) Hennigan, C. J.; Miracolo, M. A.; Engelhart, G. J.; May, A. A.; Presto, A. A.; Lee, T.; Sullivan, A. P.; McMeeking, G. R.; Coe, H.; Wold, C. E.; Hao, W. M.; Gilman, J. B.; Kuster, W. C.; De Gouw, J.; Schichtel, B. A.; Collett, J. L.; Kreidenweis, S. M.; Robinson, A. L. Chemical and Physical Transformations of Organic Aerosol from the Photo-Oxidation of Open Biomass Burning Emissions in an Environmental Chamber. *Atmos. Chem. Phys.* **2011**, *11* (15), 7669–7686.

(11) Ortega, A. M.; Day, D. A.; Cubison, M. J.; Brune, W. H.; Bon, D.; De Gouw, J. A.; Jimenez, J. L. Secondary Organic Aerosol Formation and Primary Organic Aerosol Oxidation from Biomass-Burning Smoke in a Flow Reactor during FLAME-3. *Atmos. Chem. Phys.* **2013**, *13* (22), 11551–11571.

(12) Bruns, E. A.; El Haddad, I.; Slowik, J. G.; Kilic, D.; Klein, F.; Baltensperger, U.; Prévôt, A. S. H. Identification of Significant Precursor Gases of Secondary Organic Aerosols from Residential Wood Combustion. *Sci. Rep.* **2016**, *6* (June), 1–9.

(13) Bruns, E. A.; El Haddad, I.; Keller, A.; Klein, F.; Kumar, N. K.; Pieber, S. M.; Corbin, J. C.; Slowik, J. G.; Brune, W. H.; Baltensperger, U.; Prévôt, A. S. H. Inter-Comparison of Laboratory Smog Chamber and Flow Reactor Systems on Organic Aerosol Yield and Composition. *Atmos. Meas. Tech.* **2015**, *8* (6), 2315–2332.

(14) Jaffe, D. A.; Wigder, N. L. Ozone Production from Wildfires: A Critical Review. *Atmos. Environ.* **2012**, *51*, 1–10.

(15) Brown, S. S.; Stutz, J. Nighttime Radical Observations and Chemistry. *Chem. Soc. Rev.* **2012**, *41*, 6405–6447.

(16) Wayne, R.; Barnes, I.; Biggs, P.; Burrows, J.; Canosa-Mas, C.; Hjorth, J.; Le Bras, G.; Moortgat, G.; Perner, D.; Poulet, G.; Restelli, G.; Sidebottom, H. The Nitrate Radical: Physics, Chemistry, and the Atmosphere. *Atmos. Environ., Part A* **1991**, *25* (1), 1–203.

(17) Osthoff, H. D.; Roberts, J. M.; Ravishankara, A. R.; Williams, E. J.; Lerner, B. M.; Sommariva, R.; Bates, T. S.; Coffman, D.; Quinn, P. K.; Dibb, J. E.; Stark, H.; Burkholder, J. B.; Talukdar, R. K.; Meagher, J.; Fehsenfeld, F. C.; Brown, S. S. High Levels of Nitryl Chloride in the Polluted Subtropical Marine Boundary Layer. *Nat. Geosci.* **2008**, *1* (5), 324–328.

(18) Thornton, J. A.; Kercher, J. P.; Riedel, T. P.; Wagner, N. L.; Cozic, J.; Holloway, J. S.; Dubé, W. P.; Wolfe, G. M.; Quinn, P. K.; Middlebrook, A. M.; Alexander, B.; Brown, S. S. A Large Atomic Chlorine Source Inferred from Mid-Continental Reactive Nitrogen Chemistry. *Nature* **2010**, *464* (7286), 271–274.

(19) Chang, W. L.; Bhawe, P. V.; Brown, S. S.; Riemer, N.; Stutz, J.; Dabdub, D. Heterogeneous Atmospheric Chemistry, Ambient Measurements, and Model Calculations of N<sub>2</sub>O<sub>5</sub>: A Review. *Aerosol Sci. Technol.* **2011**, *45* (6), 665–695.

(20) Ahern, A.; Goldberger, L.; Jahl, L.; Thornton, J.; Sullivan, R. C. Production of N<sub>2</sub>O<sub>5</sub> and ClNO<sub>2</sub> through Nocturnal Processing of



Biomass-Burning Aerosol. *Environ. Sci. Technol.* **2018**, *52* (2), 550–559.

(21) Hatch, L. E.; Luo, W.; Pankow, J. F.; Yokelson, R. J.; Stockwell, C. E.; Barsanti, K. C. Identification and Quantification of Gaseous Organic Compounds Emitted from Biomass Burning Using Two-Dimensional Gas Chromatography–time-of-Flight Mass Spectrometry. *Atmos. Chem. Phys.* **2015**, *15* (4), 1865–1899.

(22) Stockwell, C. E.; Yokelson, R. J.; Kreidenweis, S. M.; Robinson, A. L.; Demott, P. J.; Sullivan, R. C.; Reardon, J.; Ryan, K. C.; Griffith, D. W. T.; Stevens, L. Trace Gas Emissions from Combustion of Peat, Crop Residue, Domestic Biofuels, Grasses, and Other Fuels: Configuration and Fourier Transform Infrared (FTIR) Component of the Fourth Fire Lab at Missoula Experiment (FLAME-4). *Atmos. Chem. Phys.* **2014**, *14* (18), 9727–9754.

(23) Selimovic, V.; Yokelson, R. J.; Warneke, C.; Roberts, J. M.; de Gouw, J. A.; Griffith, D. W. T. Aerosol Optical Properties and Trace Gas Emissions from Laboratory-Simulated Western US Wildfires during FIREX. *Atmos. Chem. Phys.* **2018**, *18*, 2929–2948.

(24) Sekimoto, K.; Koss, A. R.; Gilman, J. B.; Selimovic, V.; Coggon, M. M.; Zarzana, K. J.; Yuan, B.; Lerner, B. M.; Brown, S. S.; Warneke, C.; Yokelson, R. J.; Roberts, J. M.; de Gouw, J. High- and Low-Temperature Pyrolysis Profiles Describe Volatile Organic Compound Emissions from Western US Wildfire Fuels. *Atmos. Chem. Phys. Discuss.* **2018**, 1–39.

(25) Hartikainen, A.; Yli-Pirilä, P.; Tiitta, P.; Leskinen, A.; Kortelainen, M.; Orasche, J.; Schnelle-Kreis, J.; Lehtinen, K.; Zimmermann, R.; Jokiniemi, J.; Sippula, O. Volatile Organic Compounds from Logwood Combustion: Emissions and Transformation under Dark and Photochemical Aging Conditions in a Smog Chamber. *Environ. Sci. Technol.* **2018**, *52*, 4979–4988.

(26) Atkinson, R.; Arey, J. Gas-Phase Tropospheric Chemistry of Biogenic Volatile Organic Compounds: A Review. *Atmospheric Environment*; Pergamon, 2003; Vol. 37, pp 197–219. DOI: 10.1016/S1352-2310(03)00391-1.

(27) Atkinson, R.; Arey, J. Atmospheric Degradation of Volatile Organic Compounds. *Chem. Rev.* **2003**, *103* (3), 4605–4638.

(28) Atkinson, R. Kinetics and Mechanisms of the Gas-Phase Reactions of the NO<sub>3</sub> Radical with Organic Compounds. *J. Phys. Chem. Ref. Data* **1991**, *20*, 459–507.

(29) El Zein, A.; Coeur, C.; Obeid, E.; Lauraguais, A.; Fagniez, T. Reaction Kinetics of Catechol (1,2-Benzenediol) and Guaiacol (2-Methoxyphenol) with Ozone. *J. Phys. Chem. A* **2015**, *119* (26), 6759–6765.

(30) Martínez, E.; Cabañas, B.; Aranda, A.; Martín, P.; Salgado, S. Absolute Rate Coefficients for the Gas-Phase Reactions of NO<sub>3</sub> Radical with a Series of Monoterpenes at T = 298 to 433 K. *J. Atmos. Chem.* **1999**, *33* (3), 265–282.

(31) Kerdouci, J.; Picquet-Varrault, B.; Doussin, J. F. Structure-Activity Relationship for the Gas-Phase Reactions of NO<sub>3</sub> radical with Organic Compounds: Update and Extension to Aldehydes. *Atmos. Environ.* **2014**, *84* (3), 363–372.

(32) Grosjean, D.; Williams, E. L. Environmental Persistence of Organic Compounds Estimated from Structure-Reactivity and Linear Free-Energy Relationships. Unsaturated Aliphatics. *Atmos. Environ., Part A* **1992**, *26* (8), 1395–1405.

(33) Cabañas, B.; Baeza, M. T.; Salgado, S.; Martín, P.; Taccone, R.; Martínez, E. Oxidation of Heterocycles in the Atmosphere: Kinetic Study of Their Reactions with NO<sub>3</sub> Radical. *J. Phys. Chem. A* **2004**, *108* (49), 10818–10823.

(34) Harrison, M. A. J.; Barra, S.; Borghesi, D.; Vione, D.; Arsene, C.; Iulian Olariu, R. Nitrated Phenols in the Atmosphere: A Review. *Atmos. Environ.* **2005**, *39*, 231–248.

(35) Laskin, A.; Laskin, J.; Nizkorodov, S. A. Chemistry of Atmospheric Brown Carbon. *Chem. Rev.* **2015**, *115* (10), 4335–4382.

(36) Zarzana, K. J.; Min, K. E.; Washenfelder, R. A.; Kaiser, J.; Krawiec-Thayer, M.; Peischl, J.; Neuman, J. A.; Nowak, J. B.; Wagner, N. L.; Dubé, W. P.; St. Clair, J. M.; Wolfe, G. M.; Hanisco, T. F.; Keutsch, F. N.; Ryerson, T. B.; Brown, S. S. Emissions of Glyoxal and Other Carbonyl Compounds from Agricultural Biomass Burning

Plumes Sampled by Aircraft. *Environ. Sci. Technol.* **2017**, *51* (20), 11761–11770.

(37) Neuman, J. A.; Trainer, M.; Brown, S. S.; Min, K. E.; Nowak, J. B.; Parrish, D. D.; Peischl, J.; Pollack, I. B.; Roberts, J. M.; Ryerson, T. B.; Veres, P. R. HONO Emission and Production Determined from Airborne Measurements over the Southeast U.S. *J. Geophys. Res.* **2016**, *121* (15), 9237–9250.

(38) Warneke, C.; Trainer, M.; De Gouw, J. A.; Parrish, D. D.; Fahey, D. W.; Ravishankara, A. R.; Middlebrook, A. M.; Brock, C. A.; Roberts, J. M.; Brown, S. S.; Neuman, J. A.; Lerner, B. M.; Lack, D.; Law, D.; Hübler, G.; Pollack, I.; Sjostedt, S.; Ryerson, T. B.; Gilman, J. B.; Liao, J.; Holloway, J.; Peischl, J.; Nowak, J. B.; Aikin, K. C.; Min, K. E.; Washenfelder, R. A.; Graus, M. G.; Richardson, M.; Markovic, M. Z.; Wagner, N. L.; Welti, A.; Veres, P. R.; Edwards, P.; Schwarz, J. P.; Gordon, T.; Dube, W. P.; McKeen, S. A.; Brioude, J.; Ahmadov, R.; Bougiatioti, A.; Lin, J. J.; Nenes, A.; Wolfe, G. M.; Hanisco, T. F.; Lee, B. H.; Lopez-Hilfiker, F. D.; Thornton, J. A.; Keutsch, F. N.; Kaiser, J.; Mao, J.; Hatch, C. D. Instrumentation and Measurement Strategy for the NOAA SENEX Aircraft Campaign as Part of the Southeast Atmosphere Study 2013. *Atmos. Meas. Tech.* **2016**, *9* (7), 3063–3093.

(39) Brown, S. S.; Stark, H.; Ravishankara, A. R. Cavity Ring-down Spectroscopy for Atmospheric Trace Gas Detection: Application to the Nitrate Radical (NO<sub>3</sub>). *Appl. Phys. B: Lasers Opt.* **2002**, *75* (2–3), 173–182.

(40) Dubé, W. P.; Brown, S. S.; Osthoff, H. D.; Nunley, M. R.; Ciciora, S. J.; Paris, M. W.; McLaughlin, R. J.; Ravishankara, A. R. Aircraft Instrument for Simultaneous, *in Situ* Measurement of NO<sub>3</sub> and N<sub>2</sub>O<sub>5</sub> via Pulsed Cavity Ring-down Spectroscopy. *Rev. Sci. Instrum.* **2006**, *77* (3), 034101.

(41) Fuchs, H.; Dubé, W. P.; Ciciora, S. J.; Brown, S. S. Determination of Inlet Transmission and Conversion Efficiencies for *in Situ* Measurements of the Nocturnal Nitrogen Oxides, NO<sub>3</sub>, N<sub>2</sub>O<sub>5</sub> and NO<sub>2</sub>, via Pulsed Cavity Ring-down Spectroscopy. *Anal. Chem.* **2008**, *80* (15), 6010–6017.

(42) Wild, R. J.; Edwards, P. M.; Dube, W. P.; Baumann, K.; Edgerton, E. S.; Quinn, P. K.; Roberts, J. M.; Rollins, A. W.; Veres, P. R.; Warneke, C.; Williams, E. J.; Yuan, B.; Brown, S. S. A Measurement of Total Reactive Nitrogen, NO<sub>y</sub>, Together with NO<sub>2</sub>, NO, and O<sub>3</sub> via Cavity Ring-down Spectroscopy. *Environ. Sci. Technol.* **2014**, *48* (16), 9609–9615.

(43) Ryerson, T. B.; Huey, L. G.; Knapp, K.; Neuman, J. A.; Parrish, D. D.; Sueper, D. T.; Fehsenfeld, F. C. Design and Initial Characterization of an Inlet for Gas-Phase NO<sub>y</sub> Measurements from Aircraft. *J. Geophys. Res. Atmos.* **1999**, *104* (D5), 5483–5492.

(44) Brock, C. A.; Schröder, F.; Kärcher, B.; Petzold, A.; Busen, R.; Fiebig, M. Ultrafine Particle Size Distribution Measured in Aircraft Exhaust Plumes. *J. Geophys. Res.* **2000**, *105* (Vi), 26555–26567.

(45) Brock, C. A.; Cozic, J.; Bahreini, R.; Froyd, K. D.; Middlebrook, A. M.; McComiskey, A.; Brioude, J.; Cooper, O. R.; Stohl, A.; Aikin, K. C.; De Gouw, J. A.; Fahey, D. W.; Ferrare, R. A.; Gao, R. S.; Gore, K. W.; Holloway, J. S.; Hübler, G.; Jefferson, A.; Lack, D. A.; Lance, S.; Moore, R. H.; Murphy, D. M.; Nenes, A.; Novelli, P. C.; Nowak, J. B.; Ogren, J. A.; Peischl, J.; Pierce, R. B.; Pilewskie, P.; Quinn, P. K.; Ryerson, T. B.; Schmidt, K. S.; Schwarz, J. P.; Sodemann, H.; Spackman, J. R.; Stark, H.; Thomson, D. S.; Thornberry, T.; Veres, P.; Watts, L. A.; Warneke, C.; Wollny, A. G. Characteristics, Sources, and Transport of Aerosols Measured in Spring 2008 during the Aerosol, Radiation, and Cloud Processes Affecting Arctic Climate (ARCPAC) Project. *Atmos. Chem. Phys.* **2011**, *11* (6), 2423–2453.

(46) De Gouw, J.; Warneke, C. Measurements of Volatile Organic Compounds in the Earth's Atmosphere Using Proton-Transfer-Reaction Mass Spectrometry. *Mass Spectrometry Reviews*; Wiley-Blackwell, 2007; pp 223–257. DOI: 10.1002/mas.20119.

(47) Bond, T. C.; Doherty, S. J.; Fahey, D. W.; Forster, P. M.; Berntsen, T.; Deangelo, B. J.; Flanner, M. G.; Ghan, S.; Kärcher, B.; Koch, D.; Kinne, S.; Kondo, Y.; Quinn, P. K.; Sarofim, M. C.; Schultz, M. G.; Schulz, M.; Venkataraman, C.; Zhang, H.; Zhang, S.; Bellouin, N.; Guttikunda, S. K.; Hopke, P. K.; Jacobson, M. Z.; Kaiser, J. W.;

- Klimont, Z.; Lohmann, U.; Schwarz, J. P.; Shindell, D.; Storelvmo, T.; Warren, S. G.; Zender, C. S. Bounding the Role of Black Carbon in the Climate System: A Scientific Assessment. *J. Geophys. Res. Atmos.* **2013**, *118* (11), 5380–5552.
- (48) Min, K.-E.; Washenfelder, R. a.; Dubé, W. P.; Langford, a. O.; Edwards, P. M.; Zarzana, K. J.; Stutz, J.; Lu, K.; Rohrer, F.; Zhang, Y.; Brown, S. S. A Broadband Cavity Enhanced Absorption Spectrometer for Aircraft Measurements of Glyoxal, Methylglyoxal, Nitrous Acid, Nitrogen Dioxide, and Water Vapor. *Atmos. Meas. Tech.* **2016**, *9* (2), 423–440.
- (49) Zheng, W.; Flocke, F. M.; Tyndall, G. S.; Swanson, A.; Orlando, J. J.; Roberts, J. M.; Huey, L. G.; Tanner, D. J. Characterization of a Thermal Decomposition Chemical Ionization Mass Spectrometer for the Measurement of Peroxy Acyl Nitrates (PANs) in the Atmosphere. *Atmos. Chem. Phys.* **2011**, *11* (13), 6529–6547.
- (50) Schwarz, J. P.; Gao, R. S.; Fahey, D. W.; Thomson, D. S.; Watts, L. A.; Wilson, J. C.; Reeves, J. M.; Darbeheshti, M.; Baumgardner, D. G.; Kok, G. L.; Chung, S. H.; Schulz, M.; Hendricks, J.; Lauer, A.; Kärcher, B.; Slowik, J. G.; Rosenlof, K. H.; Thompson, T. L.; Langford, A. O.; Loewenstein, M.; Aikin, K. C. Single-Particle Measurements of Midlatitude Black Carbon and Light-Scattering Aerosols from the Boundary Layer to the Lower Stratosphere. *J. Geophys. Res.* **2006**, *111* (16), 1–15.
- (51) Holloway, J. S.; Jakoubek, R. O.; Parrish, D. D.; Gerbig, C.; Volz-Thomas, A.; Schmitgen, S.; Fried, A.; Wert, B.; Henry, B.; Drummond, J. R. Airborne Intercomparison of Vacuum Ultraviolet Fluorescence and Tunable Diode Laser Absorption Measurements of Tropospheric Carbon Monoxide. *J. Geophys. Res. Atmos.* **2000**, *105* (D19), 24251–24261.
- (52) Stockwell, C. E.; Veres, P. R.; Williams, J.; Yokelson, R. J. Characterization of Biomass Burning Emissions from Cooking Fires, Peat, Crop Residue, and Other Fuels with High-Resolution Proton-Transfer-Reaction Time-of-Flight Mass Spectrometry. *Atmos. Chem. Phys.* **2015**, *15* (2), 845–865.
- (53) Kerdouci, J.; Picquet-Varrault, B.; Doussin, J. F. Prediction of Rate Constants for Gas-Phase Reactions of Nitrate Radical with Organic Compounds: A New Structure-Activity Relationship. *ChemPhysChem* **2010**, *11* (18), 3909–3920.
- (54) Edwards, P. M.; Aikin, K. C.; Dube, W. P.; Fry, J. L.; Gilman, J. B.; De Gouw, J. A.; Graus, M. G.; Hanisco, T. F.; Holloway, J.; Hübler, G.; Kaiser, J.; Keutsch, F. N.; Lerner, B. M.; Neuman, J. A.; Parrish, D. D.; Peischl, J.; Pollack, I. B.; Ravishankara, A. R.; Roberts, J. M.; Ryerson, T. B.; Trainer, M.; Veres, P. R.; Wolfe, G. M.; Warneke, C.; Brown, S. S. Transition from High- to Low-NO<sub>x</sub> Control of Night-Time Oxidation in the Southeastern US. *Nat. Geosci.* **2017**, *10* (7), 490–495.
- (55) Wolfe, G. M.; Marvin, M. R.; Roberts, S. J.; Travis, K. R.; Liao, J. The Framework for 0-D Atmospheric Modeling (FOAM) v3.1. *Geosci. Model Dev.* **2016**, *9* (9), 3309–3319.
- (56) Jenkin, M. E.; Saunders, S. M.; Pilling, M. J. The Tropospheric Degradation of Volatile Organic Compounds: A Protocol for Mechanism Development. *Atmos. Environ.* **1997**, *31* (1), 81–104.
- (57) Jenkin, M. E.; Saunders, S. M.; Wagner, V.; Pilling, M. J. Protocol for the Development of the Master Chemical Mechanism, MCM v3 (Part B): Tropospheric Degradation of Aromatic Volatile Organic Compounds. *Atmos. Chem. Phys.* **2003**, *3* (1), 181–193.
- (58) Bloss, C.; Wagner, V.; Jenkin, M. E.; Volkamer, R.; Bloss, W. J.; Lee, J. D.; Heard, D. E.; Wirtz, K.; Martin-Reviejo, M.; Rea, G.; Wenger, J. C.; Pilling, M. J. Development of a Detailed Chemical Mechanism (MCMv3.1) for the Atmospheric Oxidation of Aromatic Hydrocarbons. *Atmos. Chem. Phys.* **2005**, *5* (3), 641–664.
- (59) Jenkin, M. E.; Wyche, K. P.; Evans, C. J.; Carr, T.; Monks, P. S.; Alfara, M. R.; Barley, M. H.; McFiggans, G. B.; Young, J. C.; Rickard, A. R. Development and Chamber Evaluation of the MCM v3.2 Degradation Scheme for  $\beta$ -Caryophyllene. *Atmos. Chem. Phys.* **2012**, *12* (11), 5275–5308.
- (60) Jenkin, M. E.; Young, J. C.; Rickard, A. R. The MCM v3.3.1 Degradation Scheme for Isoprene. *Atmos. Chem. Phys.* **2015**, *15* (20), 11433–11459.
- (61) Yang, B.; Zhang, H.; Wang, Y.; Zhang, P.; Shu, J.; Sun, W.; Ma, P. Experimental and Theoretical Studies on Gas-Phase Reactions of NO<sub>3</sub> Radicals with Three Methoxyphenols: Guaiacol, Creosol, and Syringol. *Atmos. Environ.* **2016**, *125* (3), 243–251.
- (62) Tapia, A.; Villanueva, F.; Salgado, M. S.; Cabañas, B.; Martínez, E.; Martín, P. Atmospheric Degradation of 3-Methylfuran: Kinetic and Products Study. *Atmos. Chem. Phys.* **2011**, *11* (7), 3227–3241.
- (63) Lauraguais, A.; El Zein, A.; Coeur, C.; Obeid, E.; Cassez, A.; Rayez, M.-T.; Rayez, J.-C. Kinetic Study of the Gas-Phase Reactions of Nitrate Radicals with Methoxyphenol Compounds: Experimental and Theoretical Approaches. *J. Phys. Chem. A* **2016**, *120* (17), 2691–2699.
- (64) CropScape - NASS CDL Program <https://nassgeodata.gmu.edu/CropScape/> (accessed Aug 6, 2018).
- (65) Brown, S. Absorption Spectroscopy in High Finesse Cavities for Atmospheric Studies. *Chem. Rev.* **2003**, *103*, 5219.
- (66) Brown, S. S.; Stark, H.; Ravishankara, A. R. Applicability of the Steady State Approximation to the Interpretation of Atmospheric Observations of NO<sub>3</sub> and N<sub>2</sub>O<sub>5</sub>. *J. Geophys. Res.* **2003**, *108* (D17), 4539.
- (67) Olariu, R. I.; Bejan, I.; Barnes, I.; Klotz, B.; Becker, K. H.; Wirtz, K. Rate Coefficients for the Gas-Phase Reaction of NO<sub>3</sub> Radicals with Selected Dihydroxybenzenes. *Int. J. Chem. Kinet.* **2004**, *36* (11), 577–583.
- (68) Finewax, Z.; De Gouw, J. A.; Ziemann, P. J. Identification and Quantification of 4-Nitrocatechol Formed from OH and NO<sub>3</sub>-radical-Initiated Reactions of Catechol in Air in the Presence of NO<sub>x</sub>: Implications for Secondary Organic Aerosol Formation from Biomass Burning. *Environ. Sci. Technol.* **2018**, *52* (4), 1981–1989.
- (69) Desyaterik, Y.; Sun, Y.; Shen, X.; Lee, T.; Wang, X.; Wang, T.; Collett, J. L. Speciation of “Brown” Carbon in Cloud Water Impacted by Agricultural Biomass Burning in Eastern China. *J. Geophys. Res. Atmos.* **2013**, *118* (13), 7389–7399.
- (70) Claeys, M.; Vermeylen, R.; Yasmeeen, F.; Gómez-González, Y.; Chi, X.; Maenhaut, W.; Mészáros, T.; Salma, I. Chemical Characterisation of Humic-like Substances from Urban, Rural and Tropical Biomass Burning Environments Using Liquid Chromatography with UV/Vis Photodiode Array Detection and Electrospray Ionisation Mass Spectrometry. *Environ. Chem.* **2012**, *9* (3), 273–284.
- (71) Lin, P.; Bluvshstein, N.; Rudich, Y.; Nizkorodov, S. A.; Laskin, J.; Laskin, A. Molecular Chemistry of Atmospheric Brown Carbon Inferred from a Nationwide Biomass Burning Event. *Environ. Sci. Technol.* **2017**, *51* (20), 11561–11570.
- (72) Iinuma, Y.; Böge, O.; Gräfe, R.; Herrmann, H. Methyl-Nitrocatechols: Atmospheric Tracer Compounds for Biomass Burning Secondary Organic Aerosols. *Environ. Sci. Technol.* **2010**, *44*, 8453–8459.
- (73) Gaston, C. J.; Lopez-Hilfiker, F. D.; Whybrew, L. E.; Hadley, O.; McNair, F.; Gao, H.; Jaffe, D. A.; Thornton, J. A. Online Molecular Characterization of Fine Particulate Matter in Port Angeles, WA: Evidence for a Major Impact from Residential Wood Smoke. *Atmos. Environ.* **2016**, *138*, 99–107.
- (74) Mohr, C.; Lopez-Hilfiker, F. D.; Zotter, P.; Prévôt, A. S. H.; Xu, L.; Ng, N. L.; Herndon, S. C.; Williams, L. R.; Franklin, J. P.; Zahniser, M. S.; Worsnop, D. R.; Knighton, W. B.; Aiken, A. C.; Gorkowski, K. J.; Dubey, M. K.; Allan, J. D.; Thornton, J. A. Contribution of Nitrated Phenols to Wood Burning Brown Carbon Light Absorption in Detling, United Kingdom during Winter Time. *Environ. Sci. Technol.* **2013**, *47* (12), 6316–6324.
- (75) Xie, M.; Chen, X.; Hays, M. D.; Lewandowski, M.; Offenberg, J.; Kleindienst, T. E.; Holder, A. L. Light Absorption of Secondary Organic Aerosol: Composition and Contribution of Nitroaromatic Compounds. *Environ. Sci. Technol.* **2017**, *51* (20), 11607–11616.
- (76) Hinrichs, R. Z.; Buczek, P.; Trivedi, J. J. Solar Absorption by Aerosol-Bound Nitrophenols Compared to Aqueous and Gaseous Nitrophenols. *Environ. Sci. Technol.* **2016**, *50* (11), S661–S667.
- (77) Odum, J. R.; Hoffmann, T.; Bowman, F.; Collins, D.; Flagan, R. C.; Seinfeld, J. H. Gas Particle Partitioning and Secondary Organic Aerosol Yields. *Environ. Sci. Technol.* **1996**, *30* (8), 2580–2585.